Theory of optical properties of segregated InAs/GaSb superlattices

R. Magri and A. Zunger

Abstract: The authors study the effects of interfacial atomic segregation on the electronic and optical properties of InAs/GaSb superlattices. They describe their atomistic empirical pseudo-potential method and test its performance against the available experimental data. They show its ability to predict the band structure dependence on the detailed atomic configuration, and thus to properly account for the effects of interfacial atomic segregation and structural disorder. They also show how their method avoids the approximations underlying the pseudopotential method of Dente and Tilton, which gives different results. The application of the proposed method to the InAs/GaSb superlattices allows the explanation of some observed experimental results, such as: the bandgap difference between $(InAs)_8/(GaSb)_8$ superlattices with almost pure InSb-like or GaAs-like interfaces; the large blue shift of the bandgap when the growth temperature of the superlattice increases; and the blue shift of the bandgap of $(InAs)_8/(GaSb)_n$ superlattices with increasing GaSb period n. They present a detailed comparison of their predicted blue shift with that obtained by other theories.

1 Introduction

The conduction band minimum of InAs is $\sim$175 meV below the valence band maximum of GaSb. Because of its unique type of band alignment, the InAs/GaSb system permits the tuning of the effective bandgap from the mid- to the far-infrared regions by modulating the thicknesses of the InAs and GaSb layers. The tunability of the bandgap has made this system technologically interesting for infrared lasers and detectors [1]. Unfortunately, the spatial separation of carriers in type II structures decreases the hole and electron wave-function overlap and, as a consequence, decreases the radiative recombination efficiency. Thus, thin period super-lattices, which provide a larger wavefunction overlap compared to uncoupled quantum well structures, have been proposed for optoelectronic applications.

Unfortunately, the use of thin layer structures demands a much higher control over the interface morphology of the grown devices. In no-common atom heterojunctions, such as InAs/GaSb, where both the cation and anion change, the interfacial region presents four different kind of bonds: the In-As and Ga-Sb bonds of the two bulk compounds, and also the interface specific In-Sb and Ga-As bonds. The real interface atomic structure is even more complex: deviations from the ideal abrupt geometry are always present due to segregation, diffusion and exchanges with the molecular/vapour phases – all

processes related to the growth kinetic. Recent cross-sectional scanning tunnelling microscopy measurements on InAs/InGaSb superlattices have indeed observed Sb penetration into InAs, and As penetration into the first few layers of InGaSb [2, 3].

Other recent experimental results have highlighted the importance of the interface morphology on the electronic properties of the InAs/GaSb system. Yang *et al.* [4, 5] found a 30–40 meV increase of the bandgap of an $(InAs)_{5.5}/(In_{0.28}Ga_{0.72}Sb)_{10}/(InAs)_{5.5}/(AlSb)_{14}$ structure, proposed for a diode laser, when the layer thicknesses were kept constant but the growth temperature of the device was increased from 460 to 500°C. This suggests that interdiffusion changes the bandgap. Also, Vurgaftman *et al.* [6] showed that there are conspicous differences between the bandgaps (or, via a $\mathbf{k} \cdot \mathbf{p}$ fit, between the band offsets that yield those gaps) derived using data from different growers. They found differences as large as 100 meV for structures nominally identical. Bennett *et al.* [7] measured the bandgaps of InAs/GaSb superlattices with almost pure InSb-like or GaAs-like interfaces and found a difference of 40 meV for superlattices with nominal period $n = 8$. In particular, gaps $E_g = 209$ meV and 216 meV have been measured for two samples with In-Sb-like interfaces, whereas a gap $E_g = 253$ meV was measured for a sample with only GaAs-like interfaces. Clearly, the atomic-level structure at the interface controls the bandgap.

Device optimisation relies on theories capable of predicting with sufficient accuracy the interband and the intersub-band transition energies and probabilities. For thin-layer GaSb/InAs structures this is particularly challenging, because of the large dependence of the transition energies on the microscopic atomic structure of the system. We have previously shown [8] that the 'standard model' based on continuum-like effective-mass $\mathbf{k} \cdot \mathbf{p}$ approaches is insufficient to describe the electronic structure of such thin superlattices, even if they are assumed to be abrupt. A good theory should take into account the effects on the band

structure of segregation and interfacial atomic intermixing to provide accurate values.

In this paper we show that an atomistic empirical pseudopotential approach, fitted to bulk reference systems, is sensitive to the microscopical details of the atomic configuration of the system and, thus, provides an appropriate description of the electronic structure of abrupt and segregated InAs/GaSb thin layer superlattices.

2 Physically mandated requirements from an appropriate theoretical model

In selecting an appropriate theoretical approach for this system, one has to bear in mind a few basic features:

(*a*) The absence of a common-atom in InAs/GaSb geometrically mandates that (001) heterostructures will have four (not two) types of bonds. For example, the interface formed from InAs-on-GaSb has the layer sequence

$$\ldots -Sb-Ga-Sb-\mathbf{Ga}-\mathbf{As}-In-As-In-\ldots$$

$$(\text{InAs-on-GaSb}) \qquad (1)$$

whereas the GaSb-on-InAs interface has the layer sequence

$$\ldots -As-In-As-\mathbf{In}-\mathbf{Sb}-Ga-Sb-Ga\ldots$$

$$(\text{GaSb-on-InAs}) \qquad (2)$$

Thus, not only are In−As and Ga−Sb bonds present, but also Ga−As and In−Sb. This distinguishes these systems from common-atom heterostructures such as InAs/GaAs, where only the bonds present in the binary constituents are present in the heterostructure. The geometric consequence of (1) and (2) is that the point group symmetry is reduced from D2d (InAs/GaAs) to C2v (InAs/GaSb). The optical consequence is that in D2d the valence to conduction transitions have a different matrix element in the two in-plane directions [110] and [−110], i.e. the in-plane polarisation ratio, $\lambda = (P_{110} - P_{-110})/(P_{110} + P_{-110})$, (*P* dipole matrix element), is different from 1. Such anisotropies were seen experimentally in high quality no-common-atom SLs, e.g. GaInAs/InP and AlInAs/InP [9, 10]. The unavoidable consequence of the geometrical facts (1) and (2) is that an appropriate theory must represent four types of bonds, or else the physical symmetry and qualitative optical response would be incorrect.

(*b*) Since we are dealing with rather short-period super-lattices, the distance of a given layer from the interfaces will determine the potential at that layer. Thus, InAs monolayers that are distant from the interface may feel a bulk-like InAs potential, yet InAs monolayers closer to the interface will feel a surface-modified potential. This effect is evident if one examines the in-plane averaged, self-consistent potential obtained in *ab-initio* LDA calculations. Figure 1 shows such a result for an $(InAs)_6/(AlSb)_6$ (001) superlattice. The thin lines denote the in-plane ($X-Y$) averaged potential $\bar{V}(z)$, whereas the bold line emphasises the potential at the two different interfaces. Close examination shows that: (i) $\bar{V}(z)$ is different for different InAs monolayers (note the dashed line), depending on their distance from the interface; and (ii) the potential at the interfaces is different from those inside the respective layers (note the bold lines). Unfortunately, self-consistent calculations such as those shown in Fig. 1 are not always practical computationally (i.e. for the small gap InAs/GaSb system), so other approaches are needed. The unavoidable consequence of the self-consistent charge transfer effects evident from
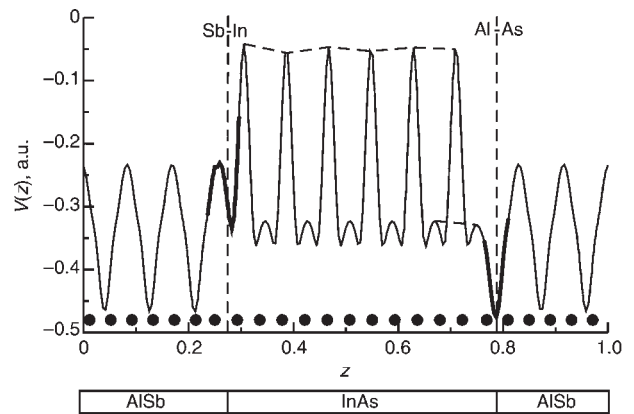

Fig. 1 *Self-consistent LDA total potential for (001) $(InAs)_6/(AlSb)_6$ superlattice in atomic units*

For comparison, the atomistic empirical pseudopotential for the (001) (InAs)/(GaSb) super-lattices is given in Fig. 3 of [25]. Note that the InAs potential is different for different InAs layers. Similarly, the two interfaces have different potentials

ab-initio calculations is that an appropriate simpler theory must allow for different effective potentials (even for chemically identical monolayers), depending on the distance to the interfaces.

(*c*) Whereas in bulk solids the effective potential $V(G)$ is defined only for bulk reciprocal lattice vectors G_{BK}, in superlattices there are nonzero values of the potential also for the reciprocal lattice vectors G_{SL} that are absent in the bulk. The values $\{V(q)\}$ for $q \neq G_{BK}$ are unimportant for the bulk solids, but they control the band structure of lower-symmetry structures, such as superlattices or random alloys. Thus, an appropriate theory of InAs/GaSb superlattices must define, in some physical manner, $V(q)$ for $q \neq G_{BK}$.

3 Dente and Tilton's approach

Dente and Tilton [11, 12] have taken a significant step beyond the continuum 'standard model', utilising empirical pseudopotentials and obtaining good results for the bandgaps of various InAs/GaSb superlattices (SLs). Their approach was different from previous atomistic pseudo-potential approaches [13−15] and from the present approach.

(*a*) Much like the $\mathbf{k} \cdot \mathbf{p}$, their approach ignores the existence of interfacial bonds in a no-common atom SL, assuming instead that the InAs potential reaches the interface, at which point the GaSb potential starts abruptly. Since no Ga−As and In−Sb bonds exist, this leads to the incorrect point-group symmetry (D2d, rather than C2v) and to an incorrect in-plane polarisation ratio $\lambda = 1$.

(*b*) Dente and Tilton assume that the potentials of all InAs monolayers are equal to each other, irrespective of the distance to the interface, and so are the potentials of all GaSb monolayers (see Fig. 1 of [11]). This requires some unusual charge redistribution whose existence is not supported by self-consistent *ab-initio* calculations (see Fig. 1 here).

(*c*) The potentials $V(q)$ at $q \neq G_{BK}$ that are required by the SL's calculations are determined implicitly by selecting one numerical 'smoothing function' rect(z/w) (see equation (1) in [11]). This procedure introduces some uncontrolled elements. Indeed, the shape of the smoothing function is unspecified, as is the question of where is the edge of the truncation (in the middle plane between two atoms?). Implicitly, the specification of the shape, number of Fourier components and origin of these functions is equivalent to a

significant set of parameters that needs somehow to be fixed. Indeed, Dente and Tilton adjust the implicit parameters of their theory (in particular the number of Fourier expansion terms of the 'smoothing function'), for abrupt SLs so as to reproduce the bandgaps of actual, non-abrupt SLs. It is thus not clear if the potential form factors $V(q \neq G_{BK})$ determined in this way implicitly can carry any independent physical significance in the case of the electronic structure of InAs/GaSb ternary and quaternary alloy systems.

(d) The procedure of Dente and Tilton does not allow considering atomistic patterns of interfacial intermixing such as those observed by X-STM [3] in InAs/GaInSb, which lead to significant changes in the bandgaps.

The atomistic model we propose [16] overcomes the four difficulties encountered above.

4 Method

Our empirical pseudopotential approach is fully atomistic. We solve the single-particle Schrödinger equation:

$$\left[-\frac{\beta}{2}\nabla^2 + \sum_{n\alpha} v_\alpha(r - R_{n\alpha}) \right] \psi_i(r) = \epsilon_i \psi_i(r) \qquad (3)$$

where $R_{n\alpha}$ denotes the position of the nth ion of type $\alpha(= \text{In, Ga, As, Sb})$. Thus, the crystal potential is written as a superposition of atomic potentials, v_α, centred around the atomic sites. The potential includes the spin–orbit interaction; thus the wavefunctions $\psi_i(r)$ are spinors with spin-up and spin-down components. For the potential v_α we do not use the local density approximation (LDA), since not only does it produce the well-known [17] LDA errors in bandgaps, but also the all-important effective masses are considerably in error, but atomic screened pseudo-potentials. In the traditional implementations of the empirical pseudopotential method the crystal potential is written in terms of few form factors $V(G)$ relative to the reciprocal lattice vectors G_i of the binary bulk solids, whereas applications to nanostructures and alloys, which have much larger unit cells, require the determination of $V(G)$ at many intermediate values. We address this point by determining the atomic screened pseudopotential form factors $v_\alpha(q)$ as a continuous function of momentum q, for the atomic species $\alpha = \text{Ga, Sb, In, As}$ of the quaternary GaSb/InAs system. We fit the parameters entering the expression for the form factors to the experimentally measured electron and hole effective masses, bandgaps (target values at 0 K), spin–orbit splittings, hydrostatic deformation potentials of the bandgaps, band offsets [18, 19], and LDA-predicted single band edge deformation potentials [20] of the four binary systems. The results of the fit are given elsewhere [16].

The term β, which scales the kinetic energy in the Schrödinger equation, has been introduced to represent the quasiparticle nonlocal self-energy effects [21]. In fact, it can be shown that at the lowest order, the leading effects of the non-local many body potential can be represented by scaling the kinetic energy [22]. This kinetic energy scaling is needed to simultaneously fit bulk effective masses and bandgaps.

Also, the traditional form of the empirical pseudopotential approach is strain-independent. Thus, the dependence of the valence band maximum and conduction band minimum on the hydrostatic deformations was discovered often to have the incorrect sign. To obtain the correct behaviour of the band-edge energies under hydrostatic or biaxial strain deformations we have built the response to the strain

directly into the screened atomic pseudopotetials v_α, adding an explicit strain dependent term $\delta v_\alpha(\epsilon)$. This term plays a crucial role in describing the variation of the valence band-edge and, separately, the conduction band-edge under arbitrary strains. This allows us to describe the modification of the valence and conduction band offsets when the systems are subjected to hydrostatic or biaxial deformation conditions such as in the case of epitaxial growth on a lattice-mismatched substrate. Note that, even though the binary GaSb and InAs systems are nearly lattice-matched (the lattice mismatch is relatively small, 0.6%), the quaternary systems manifest at the interface also Ga–As and In–Sb bonds which have a huge mutual lattice mismatch of 14% and are also strongly mismatched (by ~ 6–7%) with respect to the Ga-Sb and In-As bonds. We fitted not only the experimental hydrostatic deformation potentials of the bandgap, but also the *ab-initio* calculated hydrostatic deformation potentials of the valence band maximum [20]. The *ab-initio* LDA based calculations have shown that the hydrostatic deformation potential of the single valence band-edge is small and negative for arsenide and antimonide III–V compounds due to the interaction between the valence band-edge states and the underlying d electrons [20]. Thus, contrary to what is usually implied, the largest contribution to the bandgap deformation potential originates from the deformation potential of the conduction band minimum, which is strongly negative.

In the InAs/GaSb system, we need to apply our scheme to different atomic local environments than those present in the fitted pure binary compounds. We address the problem considering only the nearest-neighbour environment. In the quaternary (AC)(BD) systems, the C and D anions can be surrounded by A_nB_{4-n} cations, where $n = 0, 1, 2, 3$ and 4. Analogously, the A and B cations can be surrounded by C_nD_{4-n} anions. Our EPM has been obtained by fitting the properties of only the pure binary compounds (corresponding to environments $n = 0$ and $n = 4$). To improve the transferability to other environments, we assume a linear interpolation between these limits as:

$$v_A(C_nD_{4-n}) = \frac{n}{4}v_A(AC) + \frac{4-n}{4}v_A(AD)$$

$$v_B(C_nD_{4-n}) = \frac{n}{4}v_B(BC) + \frac{4-n}{4}v_B(BD)$$

$$v_C(A_nB_{4-n}) = \frac{n}{4}v_C(AC) + \frac{4-n}{4}v_C(BC)$$

$$v_D(A_nB_{4-n}) = \frac{n}{4}v_D(AD) + \frac{4-n}{4}v_D(BD) \qquad (4)$$

AC, BC, AD and BD are the four binary compounds – in our case GaSb, GaAs, InSb and InAs – whose properties have been directly fitted to extract the atomic pseudo-potential parameters.

An empirical pseudopotential calculation requires: (a) to determine a reliable equilibrium atomic configuration for the system, and (b) to calculate the band structure relative to that given atomic configuration. To determine the atomic positions $R_{n\alpha}$ in the Schrödinger equation, we minimise the elastic energy corresponding to a given atomic arrangement in the system, via the valence force field approach [23]. For (b) we expand the wavefunctions $\psi_i(r)$ in a plane wave basis. The Hamiltonian matrix elements are calculated in this basis with no approximation; then the Hamiltonian matrix is diagonalised via the folded spectrum method [24].

Our construction satisfies the conditions set for SL calculations (see Section 2): (i) the use of atomic resolution in the potential (3) naturally allows for all (four) types of chemical bonds to be present; (ii) the superposition principle

underlying (3) naturally allows for the potential of the various InAs monolayers to differ from each other, depending on their distance from the interface. This is clearly shown in Fig. 3 of [25], where the potential of InAs is similar to the self-consistent one (Fig. 1 here); (iii) the form factors $V(\mathbf{q} \neq \mathbf{G}_{BK})$ are determined explicitly by fitting many properties of bulk materials at different volumes; (iv) interdiffused interfaces are described in a simple way.

We next test the performance of our empirical pseudo-potential description against the available experimental results.

5 Results

5.1 Band bowing of ternary alloys

An important test of the capability of our scheme to treat disorder effects properly in the quaternary InAs/GaSb system is the prediction of the band bowings of all the ternary alloys. The ternary random $In_xGa_{1-x}As$, $In_xGa_{1-x}Sb$, $GaAs_{1-x}Sb_x$ and $InAs_{1-x}Sb_x$ alloys are modelled by occupying randomly the sites of a 512 atom cubic supercell for compositions $x = 0.25$, 0.50 and 0.75. For each alloy configuration, the atomic positions were relaxed using the valence force field (VFF) method [23], while the supercell size is determined by a lattice constant given by the composition average of the lattice constants of the consituent binary compounds following Vegard's law. The calculated optical band bowings are correctly predicted positive, and in the case of the $InAs_{1-x}Sb_x$ ternary alloy we find the absolute minimum gap around $x = 0.5$ to be in good agreement with experiment [18, 19]. In Fig. 2 we show the dependence of the bandgaps of the ternary alloys against composition. We obtain the following bowing parameters: for the $In_{0.5}Ga_{0.5}As$ alloy a value $b = 0.54$ (expt. 0.49, 0.61 [18, 19]); for the $In_{0.5}Ga_{0.5}Sb$ alloy, $b = 0.32$ (expt. 0.42 [18, 19]); for the $InAs_{0.5}Sb_{0.5}$ alloy, $b = 0.72$ (expt. 0.67 [6], 0.76 [18, 19]). Only for the $GaAs_{0.5}Sb_{0.5}$ alloy is

the calculated bowing, 0.53, definitely smaller than the experimental value, 1.0 [18, 19]. Perhaps more detailed calculations of the alloy bandgap, also taking into account ordering effects (the $GaAs_{0.5}Sb_{0.5}$ alloy is known indeed to present spontaneous ordering in the chalcopyrite structure, which lowers the fundamental gap considerably), need to be performed.

We stress here that the bandgaps of the alloys have not been fitted. Differently from other methods [11, 12], where new sets of parameters must be determined for each alloy system and for each alloy composition, here we have obtained the bandgaps of all the ternary alloys at all compositions, having fitted only the binary compounds.

5.2 Interface-composition dependence of bandgaps of $(InAs)_8/(GaSb)_8$ superlattices

We have calculated the value of the fundamental bandgap of the $(InAs)_8/(GaSb)_8$ SLs, where we have changed the composition of the interface bonds in an otherwise ideal abrupt structure, by swapping only one interface anion plane from Sb to As, or vice versa. In this way we end up with a $(InAs)_{7.5}/(GaSb)_{8.5}$ superlattice with two In–Sb interfaces and a $(InAs)_{8.5}/(GaSb)_{7.5}$ superlattice with two Ga–As interfaces. The calculated bandgaps are $E_g = 229$ meV for the structure with two In–Sb interfaces, $E_g = 279$ meV for the structure with two Ga–As interfaces and $E_g = 238$ meV for the structure with one In–Sb interface and one Ga–As interface. We can compare these values with the experimental results. The measured bandgaps are $E_g^{expt} = 209$ and 216 meV for two different structures with two InSb interfaces, and $E_g^{expt} = 253$ meV for the structure with two Ga–As interfaces [7]. The superlattices with a larger number of Ga–As interfacial bonds are correctly predicted to have a higher bandgap. Moreover, the calculated value of the difference between the bandgaps, 50 meV, compares well with the measured value, 40 meV.
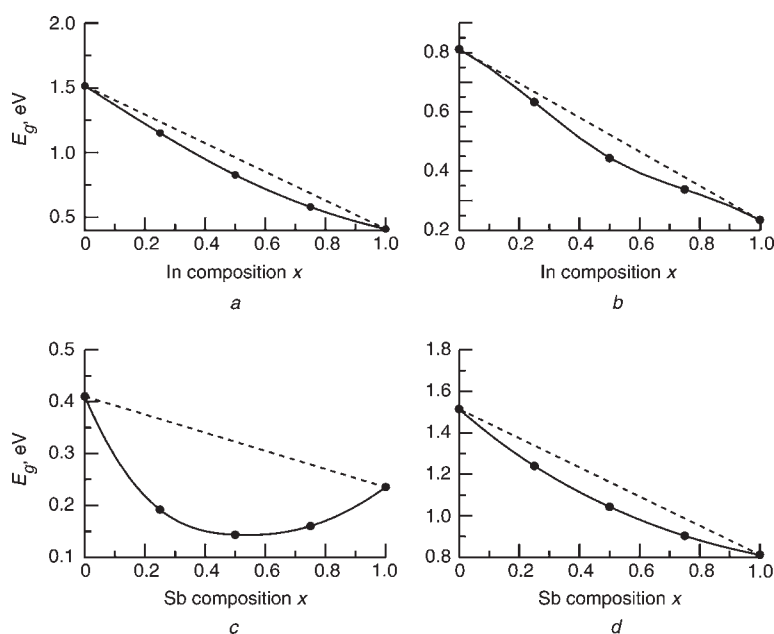

Fig. 2 *Calculated bandgaps of ternary alloys against composition x*
Dashed lines indicate linear weighted averages
a $Ga_{1-x}In_xAs$
b $Ga_{1-x}In_xSb$
c $InAs_{1-x}Sb_x$
d $GaAs_{1-x}Sb_x$

5.3 Blue shift of bandgap of segregated InAs/GaSb superlattices against ideal structures

To describe interfacial segregation effects we need a realistic model of the atomistic structure of segregated InAs/GaSb SLs. To obtain it we relied on a kinetic model for molecular beam epitaxy (MBE) growth first introduced by Dehaese *et al.* [26]. We extended the model to treat the simultaneous segregation of group III and group V species in the no-common atom InAs/GaSb system. Details of our kinetic model are given elsewhere [25]. Segregation is driven by atomic exchange between atoms in the subsurface monolayer and atoms at the surface. The exchange rate depends on the growth temperature and on the overcoming of a net energy barrier for atomic swapping between the surface and the subsurface layers, which depends on the kind of atom. For the In and Ga cations, appropriate values for the exchange energies have been reported in previous papers [26], while for the Sb and As anions we have extracted them by fitting our growth model to the Sb concentration profiles measured via cross-sectional STM [2, 3]. The fit has been described in [25].

The growth model correctly shows that Sb segregates into the InAs layer and that In segregates into the GaSb layer as observed experimentally [2, 3]. It also predicts the unexpected penetration of As into the first two layers of GaSb, in agreement with recent experimental finding [27]. Through the kinetic model of MBE growth we can obtain realistic composition profiles for the superlattices along the growth direction. Next, we need to build their atomistic structure. No experimental information is available on the atomistic arrangement in the planes perpendicular to the growth direction. We thus assume random arrangements in these planes, consistent with the planar composition profile dictated by the growth model. Once we have determined the superlattice configuration at a given growth temperature T_g, we allow local atomic displacements minimising the strain energy of the structure using a valence force field approach [23].

Finally, we apply our atomistic empirical pseudopotential technique to assess the effects on the band structure of the segregation at different growth temperatures, T_g. Figure 3 shows the trend of the bandgaps as a function of the superlattice growth temperature T_g for $(InAs)_8/(GaSb)_8$ and $(InAs)_8/(GaSb)_{16}$. In the Figure we also report
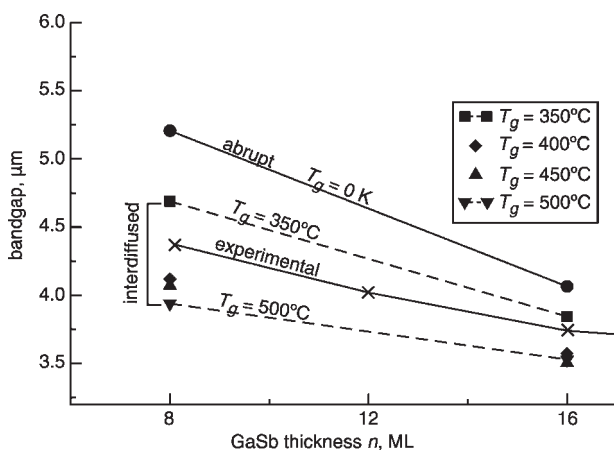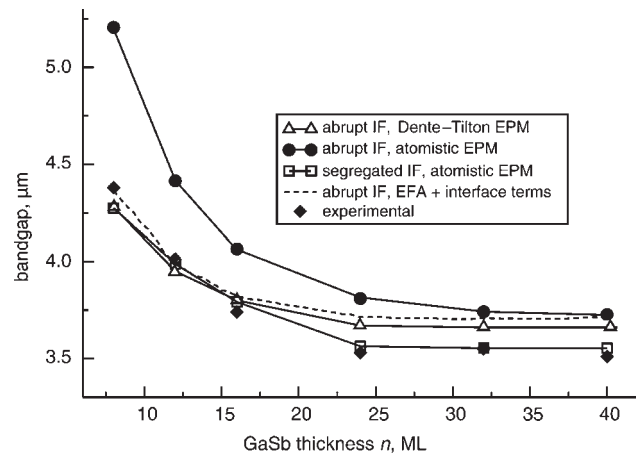

Fig. 4 *Comparison between predictions for bandgaps of $(InAs)_8/(GaSb)_n$ superlattices given by EPM method of Dente et al., by EFA method plus interface terms (see [30]) and by our method for superlattices with abrupt interfaces and segregated interfaces*

Experimental data of Kaspi *et al.* [21] are reported in the figure (full diamonds). The lines are guidelines for the eye

the experimental bandgaps as deduced from the absorbance data of Kaspi *et al.* [28, 29] for the $(InAs)_8/(GaSb)_n$ SLs. We see that abrupt SLs produce significantly (up to 50 meV) smaller gaps than SLs with intermixed interfaces. Since interfacial mixing is a fact (X-STM), one must compute bandgaps of nonideal interfaces. The blue shift of the bandgaps with increasing sample growth temperature is in agreement with the trend observed recently by Yang *et al.* [4, 5]. The bandgap wavelength decrease (blue shift) with T_g is larger for the $(InAs)_8/(GaSb)_8$ SL than for the $(InAs)_8/(GaSb)_{16}$ SL, and also the difference between the bandgap wavelength of the ideal abrupt geometry and that of the segregated ones is larger for the $(InAs)_8/(GaSb)_8$ SL.

In Fig. 4 we compare our results for the bandgaps of the $(InAs)_8/(GaSb)_n$ SLs with abrupt and segregated interfaces with those predicted by other calculations. We note the following features:

(i) assuming artificially abrupt interfaces, our atomistic empirical pseudopotential approach predicts much smaller bandgaps than does the Dente and Tilton [11, 12] empirical pseudopotential approach. Since the pseudopotentials are similar for the bulk solids, the Dente–Tilton approach involves for SLs some approximations about the interface structure not done in the atomistic approach, (see Section 3). (ii) The envelope function calculation by Lau and Flatte [30] with interfacial terms added to optimise the agreement with the experiment fits the experiment well for $n \lesssim 16$ and at larger n approaches our result for the bandgaps of abrupt interfaces. However, this approach is not predictive and it does not allow for easy inclusion of the segregation effects. (iii) The atomistic pseudopotential with segregated interfaces (obtained for a growth temperature $T_g = 400°C$ and a deposition rate of 1 ML/s) fits the experiment well. Since interfacial intermixing is an experimental fact, the agreement of the theory for intermixed SLs with the experiment is gratifying. (iv) As for the comparison of blue shifts, the predicted blue shift of the bandgap is only 47 meV for the EFA approach and 49 meV for the pseudopotential approach of Dente and Tilton [11, 12], smaller than the experimental value, 70 meV, and smaller also than our predicted blue shifts for the same SLs with segregated interfaces, 64 meV, and with abrupt interfaces, 95 meV.

Fig. 3 *Blue shift of bandgap of $(InAs)_8/(GaSb)_8$ and $(InAs)_8/(GaSb)_{16}$ superlattices with increasing growth temperature T_g*

Experimental bandgaps deduced from absorbance data of Kaspi *et al.* [28, 29] are given for comparison (crosses)
Growth rate: 0.25 ML/s

6 Conclusions

We have presented in this paper a fully atomistic approach to band structure calculations based on an empirical pesudopotential method and integrating new features such as: (i) a consistent treatment of the local strain around the atoms and in the structure; (ii) an appropriate description of all the bonds present in the quaternary InAs/GaSb system, not only the bulk Ga-Sb and In-As bonds but also the interface specific bonds Ga−As and In−Sb; and (iii) an improved transferability scheme where the first neighbour environment of each atom is taken into account. We have shown that our scheme is capable of successfully describing interfacial segregation and intermixing effects in InAs/GaSb superlattices, since it possesses the necessary sensitivity to the microscopic atomic configurations in the system. Our scheme correctly reproduces trends of the fundamental gap with: (*a*) interfacial bond composition; (*b*) interfacial segregation; and (*c*) superlattice period, which have been observed experimentally.

7 Acknowledgment

8 References

1 Meyer, J.R., Olafsen, L.J., Aifer, E.H., Bewley, W.W., Felix, C.L., Vurgaftman, I., Yang, M.J., Goldberg, L., Zhang, D., Lin, C.H., Pei, S.S., and Chow, D.H.: 'Type II W, interband cascade and vertical-cavity surface-emitting mid-IR lasers', *IEE Proc., Optoelectron.*, 1998, **145**, p. 275

2 Steinshnider, J., Weimer, M., Kaspi, R., and Turner, G.W.: 'Visualizing interfacial structure at non-common-atom heterojunctions with cross-sectional scanning tunneling microscopy', *Phys. Rev. Lett.*, 2000, **85**, p. 2953

3 Steinshnider, J., Harper, J., Weimer, M., Lin, C.H., Pei, S.S., and Chow, D.H.: 'Origin of antimony segregation in GaInSb/InAs strained-layer superlattices', *Phys. Rev. Lett.*, 2000, **85**, p. 4562

4 Yang, M.J., Moore, W.J., Bennet, B.R., and Shanabrook, B.V.: 'Growth and characterisation of InAs/InGaSb/InAs/AlSb infrared laser structures', *Electron. Lett.*, 1998, **34**, p. 270

5 Yang, M.J., Moore, W.J., Bennet, B.R., Shanabrook, B.V., Cross, J.O., Bewley, W.W., Felix, C.L., Vurgaftman, I., and Meyer, J.R.: 'Optimum growth parameters for type-II infrared lasers', *J. Appl. Phys.*, 1999, **86**, p. 1796

6 Vurgaftman, I., Meyer, J.R., and Ram-Mohan, L.R.: 'Band parameters for III-V compound semiconductors and their alloys', *J. Appl. Phys.*, 2001, **89**, p. 5815

7 Bennett, B.R., Shanabrook, B.V., Wagner, R.J., Davis, J.L., Waterman, J.R., and Twigg, M.E.: 'Interface composition control in InAs/GaSb superlattices', *Solid-State Electron.*, 1994, **37**, p. 733

8 Zunger, A.: 'On the farsightedness (hyperopia) of the standard, k·p model', *Phys. Status Solidi A*, 2002, **190**, p. 467

9 Krebs, O., and Voisin, P.: 'Giant optical anisotropy of semiconductor heterostructures with no common atom and the quantum-confined Pockels effect', *Phys. Rev. Lett.*, 1996, **77**, p. 1829

10 Krebs, O., Rondi, D., Gentner, J.L., Goldstein, L., and Voisin, P.: 'Inversion asymmetry in heterostructures of zinc-blende semiconductors: interface and external potential versus bulk effects', *Phys. Rev. Lett.*, 1998, **80**, p. 5770

11 Dente, G.C., and Tilton, M.L.: 'Pseudopotential methods for superlattices: Applications to mid-infrared semiconductor lasers', *J. Appl. Phys.*, 1999, **86**, p. 1420

12 Dente, G.C., and Tilton, M.L.: 'Comparing pseudopotential predictions for InAs/GaSb superlattices', *Phys. Rev. B*, 2002, **66**, p. 165307

13 Mader, K.A., and Zunger, A.: 'Empirical atomic pseudopotentials for AlAs/GaAs superlattices, alloys, and nanostructures', *Phys. Rev. B*, 1994, **50**, p. 17393

14 Wood, D.M., and Zunger, A.: 'Successes and failures of the, k·p method: a direct assessment for GaAs/AlAs quantum structures', *Phys. Rev. B*, 1996, **53**, p. 7949

15 Wang, L.W., and Zunger, A.: 'Local-density-derived semiempirical pseudopotentials', *Phys. Rev. B*, 1995, **51**, p. 17398

16 Magri, R., and Zunger, A.: 'Effects of interfacial atomic segregation and intermixing on the electronic properties of InAs/GaSb superlattices', *Phys. Rev. B*, 2002, **65**, p. 165302

17 Perdew, J.P., and Zunger, A.: 'Self-interaction correction to density-functional approximations for many-electron systems', *Phys. Rev. B*, 1981, **23**, p. 5048

18 Madelung, O. (Ed.): 'Semiconductors: Group IV and III-V compounds' (Springer, Berlin, 1982), Landolt-Börnstein New Series, Group III, vol. 17

19 Madelung, O. (Ed.): 'Semiconductors: intrinsic properties of Group IV elements and III-V, II-VI and I-VII compounds' (Springer, Berlin, 1987), Landolt-Börnstein New Series, Group III, vol. 22

20 Wei, S.-H., and Zunger, A.: 'Calculated natural band offsets of all II-VI and III-V semiconductors: Chemical trends and the role of cation d orbitals', *Appl. Phys. Lett.*, 1998, **72**, p. 2011

21 Magri, R., Wang, L.L., Zunger, A., Vurgaftman, I., and Meyer, J.R.: 'Anticrossing semiconducting band gap in nominally semimetallic InAs/GaSb superlattices', *Phys. Rev. B*, 2000, **61**, p. 10235

22 Cohen, M., and Heine, V.: in Ehrenreich, H., Seitz, F., and Turnbull, D. (Eds.): 'Solid state physics' (Academic Press, New York, 1970), vol. 24, p. 64

23 Keating, P.N.: 'Effect of Invariance Requirements on the Elastic Strain Energy of Crystals with Applications to the Diamond Structure', *Phys. Rev.*, 1966, **145**, p. 637

24 Wang, L.W., and Zunger, A.: 'Solving Schrodinger's equation around a desired energy: application to silicon quantum dots', *J. Chem. Phys.*, 1994, **100**, p. 2394

25 Magri, R., and Zunger, A.: 'Effects of interfacial atomic segregation on optical properties of InAs/GaSb superlattices', *Phys. Rev. B*, 2001, **64**, p. 081305

26 Dehaese, O., Wallart, X., and Mollot, F.: 'Kinetic model of element III segregation during molecular beam epitaxy of III-III′-V semiconductor compounds', *Appl. Phys. Lett.*, 1995, **66**, p. 52

27 Wiemer, M., private communication

28 Kaspi, R., Moeller, C., Ongstad, A., Tilton, M.L., Gianardi, D., Dente, G., and Gopaladasu, P.: 'Absorbance spectroscopy and identification of valence subband transitions in type-II InAs/GaSb superlattices', *Appl. Phys. Lett.*, 2000, **76**, p. 409

29 Ongstad, A.P., Kaspi, R., Moeller, C.E., Tilton, M.L., Gianardi, D.M., Chavez, J.R., and Dente, G.C.: 'Spectral blueshift and improved luminescent properties with increasing GaSb layer thickness in InAs-GaSb type-II superlattices', *J. Appl. Phys.*, 2001, **89**, p. 2185

30 Lau, W.H., and Flatte, M.E.: 'Effect of interface structure on the optical properties of InAs/GaSb laser active regions', *Appl. Phys. Lett.*, 2002, **80**, p. 1683